

RESEARCH ARTICLE

10.1002/2016JC012224

Circulation and oxygen cycling in the Mediterranean Sea: Sensitivity to future climate change

Helen R. Powley¹, Michael D. Krom^{1,2,3}, and Philippe Van Cappellen¹

Key Points:

- Climate change will impact thermohaline circulation in the Mediterranean Sea
- Transfer of labile dissolved organic carbon to deep waters strongly controls oxygen distributions in the Mediterranean Sea
- Even for the most severe decline in deep water formation projected by 2100 the Mediterranean Sea water column will remain fully oxygenated

Supporting Information:

- Supporting Information S1

Correspondence to:

H. R. Powley,
hrpowley@uwaterloo.ca

Citation:

Powley, H. R., M. D. Krom, and P. Van Cappellen (2016), Circulation and oxygen cycling in the Mediterranean Sea: Sensitivity to future climate change, *J. Geophys. Res. Oceans*, 121, 8230–8247, doi:10.1002/2016JC012224.

Received 10 AUG 2016

Accepted 20 OCT 2016

Accepted article online 25 OCT 2016

Published online 12 NOV 2016

¹Ecohydrology Research Group, Water Institute and Department of Earth and Environmental Sciences, University of Waterloo, Waterloo, Ontario, Canada, ²School of Earth and Environment, University of Leeds, Leeds, UK, ³Department of Marine Biology, Charney School of Marine Sciences, University of Haifa, Haifa, Israel

Abstract Climate change is expected to increase temperatures and decrease precipitation in the Mediterranean Sea (MS) basin, causing substantial changes in the thermohaline circulation (THC) of both the Western Mediterranean Sea (WMS) and Eastern Mediterranean Sea (EMS). The exact nature of future circulation changes remains highly uncertain, however, with forecasts varying from a weakening to a strengthening of the THC. Here we assess the sensitivity of dissolved oxygen (O₂) distributions in the WMS and EMS to THC changes using a mass balance model, which represents the exchanges of O₂ between surface, intermediate, and deep water reservoirs, and through the Straits of Sicily and Gibraltar. Perturbations spanning the ranges in O₂ solubility, aerobic respiration kinetics, and THC changes projected for the year 2100 are imposed to the O₂ model. In all scenarios tested, the entire MS remains fully oxygenated after 100 years; depending on the THC regime, average deep water O₂ concentrations fall in the ranges 151–205 and 160–219 μM in the WMS and EMS, respectively. On longer timescales (>1000 years), the scenario with the largest (>74%) decline in deep water formation rate leads to deep water hypoxia in the EMS but, even then, the WMS deep water remains oxygenated. In addition, a weakening of THC may result in a negative feedback on O₂ consumption as supply of labile dissolved organic carbon to deep water decreases. Thus, it appears unlikely that climate-driven changes in THC will cause severe O₂ depletion of the deep water masses of the MS in the foreseeable future.

1. Introduction

The Mediterranean Sea (MS) basin is considered one of the world's regions most responsive to global climate change [Giorgi, 2006]. Major changes in circulation and environmental status as a result of natural climate change have punctuated the MS's recent geological past [Rohling *et al.*, 2015, and references therein]. Over the coming decades, the MS is predicted to become warmer and drier [Collins *et al.*, 2013; Kirtman *et al.*, 2013], thus increasing water column temperature and salinity [Gualdi *et al.*, 2013, and references therein]. Temperature and salinity have opposing effects on the density of water and therefore on the Mediterranean thermohaline circulation (THC). Modeling results generally predict that the THC will weaken in response to projected future climate change, with lower water flows into and out of the deep water layers [Thorpe and Bigg, 2000; Somot *et al.*, 2006; Herrmann *et al.*, 2008; Planton *et al.*, 2012]. Adloff *et al.* [2015], however, show that Mediterranean THC model responses to climate change are very sensitive to the imposed boundary conditions: depending on how the latter are formulated, predictions range from a weakening to a strengthening of the THC.

The MS has been described as a laboratory for studying environmental change in ocean systems [Bergamasco and Malanotte-Rizzoli, 2010]. Deep water (DW) temperature and salinity of the Western Mediterranean Sea (WMS) have been increasing since at least the 1960s [e.g., Béthoux *et al.*, 1990; Rixen *et al.*, 2005; Marty and Chiaverini, 2010; Borghini *et al.*, 2014], reflecting a strong coupling of water column properties to atmospheric forcing. In recent decades, a major change was detected in the circulation of the Eastern Mediterranean (EMS), with DW formation strengthening and switching location temporarily from the Adriatic Sea to the Aegean Sea, a phenomenon referred to as the Eastern Mediterranean Transient (EMT) [Roether *et al.*, 1996]. The EMT altered the salinity and heat signatures of intermediate water (IW) flowing through the Strait of Sicily [Gasparini *et al.*, 2005; Roether and Lupton, 2011], in turn triggering enhanced DW formation in the WMS between 2004 and 2006 [Schroeder *et al.*, 2006, 2008b], known as the Western Mediterranean

Transition (WMT). The EMT left distinct biogeochemical signatures on the water masses of the MS, including changes in the distributions of oxygen (O_2), phosphorus, and nitrogen [Klein *et al.*, 1999, 2003; Kress *et al.*, 2003, 2012, 2014; Powley *et al.*, 2014; Schneider *et al.*, 2014].

Dissolved O_2 is a biogeochemical master variable in marine and freshwater ecosystems. The biogeochemical cycles of carbon and nutrients are closely coupled to that of O_2 through primary production and organic matter respiration. Oxygen consumption rates in the DW of the MS are relatively high when compared to DW of the Atlantic and Pacific Oceans [Christensen *et al.*, 1989; Roether and Well, 2001]. In the MS, DW O_2 consumption is partly coupled to the respiration of dissolved organic carbon (DOC) supplied from areas of DW formation, which supplements aerobic degradation of sinking particulate organic carbon (POC) [Christensen *et al.*, 1989; Lefèvre *et al.*, 1996; Santinelli *et al.*, 2010]. At the present time, relatively high rates of DW formation and low primary productivity keep the MS well ventilated with DW O_2 saturation levels above 70%.

In this paper, we use an O_2 mass balance model coupled to a simple representation of the water cycle in the WMS and EMS to analyze the potential effects of predicted future changes in THC driven by climate change on the O_2 levels of the IW and DW masses of the MS. Specifically, we impose perturbations to the O_2 and water cycles that span the published range of changes in temperature, salinity, and circulation projected for the year 2100. The relative effects of O_2 solubility, respiration kinetics, and circulation are assessed, with particular attention given to the differences in O_2 dynamics in the WMS versus the EMS.

2. Coupled Water-Oxygen Cycling Model

2.1. Baseline Water Cycle

The water cycle model of the MS builds on that previously developed for the EMS [Van Cappellen *et al.*, 2014]. The water columns of both WMS and EMS are split into three depth intervals (Figure 1): surface water (WMSW and EMSW), intermediate water (WMIW and EMIW), and deep water (WMDW and EMDW). The water reservoirs defined in Figure 1 approximate water masses referred to by different names in the literature: WMSW and EMSW correspond roughly to Atlantic Water (AW), while Levantine Intermediate Water (LIW) is used to refer to WMIW and EMIW. Note, however, that Western Intermediate Water and Tyrrhenian Deep Water are also included in WMIW and WMDW, respectively. A detailed justification of the fluxes associated with the EMS water cycle can be found in Van Cappellen *et al.* [2014].

The MS is an evaporative basin. Long-term evaporation (E) minus precipitation (P) in the WMS is $490 \pm 7 \text{ mm yr}^{-1}$, based on data from 1948 to 2009 [Criado-Aldeanueva *et al.*, 2012]. Average riverine input (R) of freshwater into the WMS between 1960 and 2000 is estimated at $123 \pm 10 \text{ km}^3 \text{ yr}^{-1}$ [Ludwig *et al.*, 2009]. Fresh submarine groundwater discharge (SGD) for the entire MS is estimated at $68 \text{ km}^3 \text{ yr}^{-1}$ by Zekster *et al.*, [2007]. The latter authors also provide region-by-region SGD values for the MS, from which we derive a fresh SGD input to the WMS of $27 \pm 2 \text{ km}^3 \text{ yr}^{-1}$. Net evaporation (E-P-R-SGD) for the WMS is therefore $249 \pm 18 \text{ km}^3 \text{ yr}^{-1}$, or $0.008 \pm 0.0004 \text{ Sv}$ (Figure 1). In the EMS, net evaporation is estimated at 0.055 Sv (see Van Cappellen *et al.* [2014] for details).

Quantifying the flow of water through the Strait of Gibraltar is key to the water balance of the MS. Estimates of the outflow to the Atlantic Ocean range from 0.68 Sv, using direct flow measurements over the course of 1 year [Bryden *et al.*, 1994], to 1.6 Sv based on salt and heat balance calculations [Béthoux and Gentili, 1999]. Recent continuous deployments of Acoustic Doppler current profilers from 2004 to 2007 yield an outflow flux of $0.78 \pm 0.05 \text{ Sv}$ [Sánchez-Román *et al.*, 2009; Soto-Navarro *et al.*, 2010], which is the value used in our model. The net inflow of water through the Strait of Gibraltar calculated from a global freshwater balance for the MS is $0.038 \pm 0.007 \text{ Sv}$ [Soto-Navarro *et al.*, 2010]. Hence, the steady state inflow from the Atlantic Ocean must be close to $0.82 \pm 0.06 \text{ Sv}$. The final model value is adjusted to 0.83 Sv to maintain a steady state water balance for the WMSW. The water exiting the WMS through the Strait of Gibraltar is a mixture of intermediate and deep water [Millot, 2009, 2014]. Based on a recent statistical analysis of continuous pH measurements at the Espartel Sill from 2012 to 2015, Flecha *et al.* [2015] estimate that 40% of the outflow is comprised of WMDW and 60% of WMIW, in agreement with previous estimates by García Lafuente *et al.* [2007]. Imposing the same fractions in our water cycle then gives the water fluxes through the Strait of Gibraltar in Figure 1.

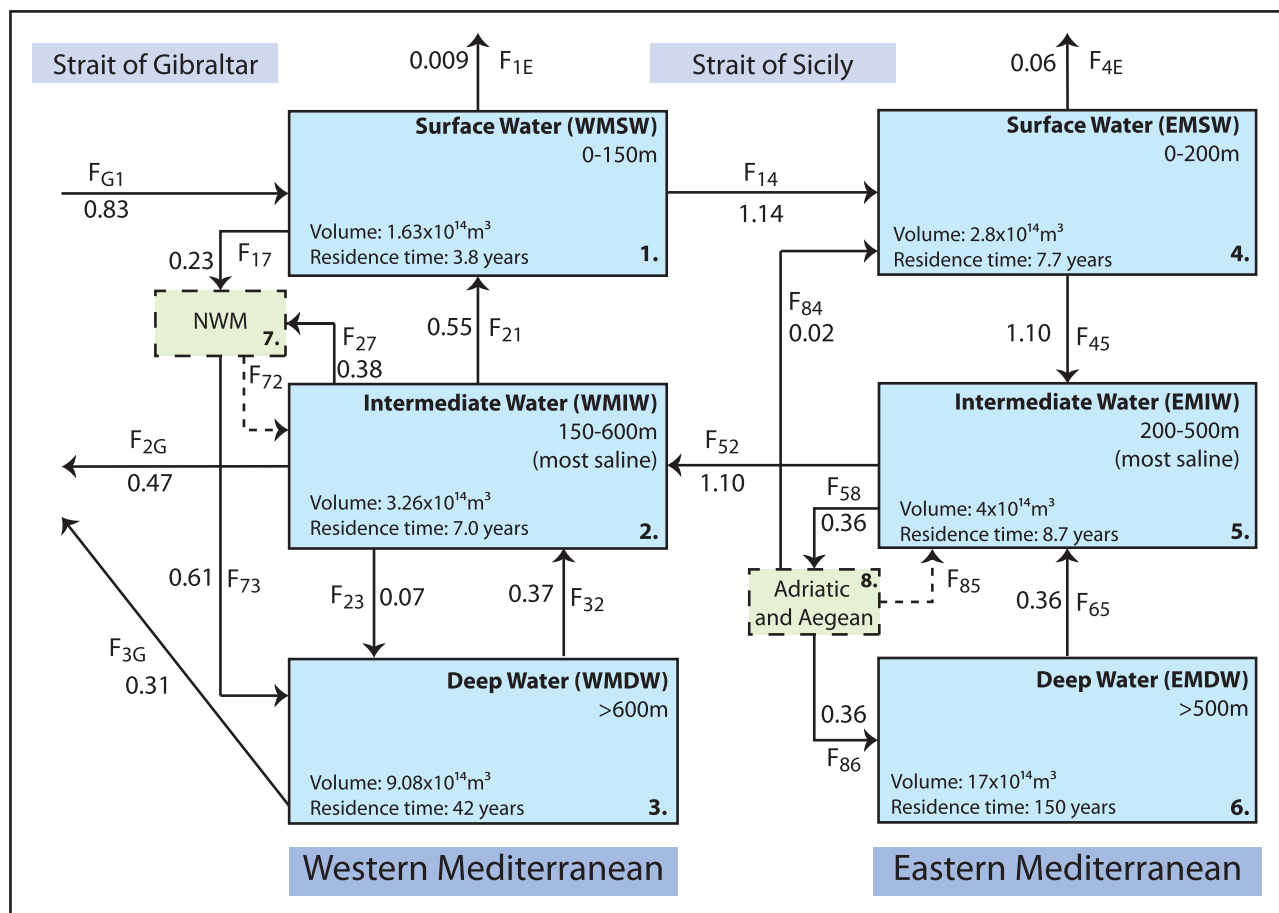


Figure 1. Water cycle model. Reservoir volumes assume WMS and EMS surface areas of $815 \times 10^3 \text{ km}^2$ and $1336 \times 10^3 \text{ km}^2$, respectively. Fluxes are given in Sv ($10^6 \text{ m}^3 \text{ s}^{-1}$). The North-West Mediterranean (NWM) represents the area where DW formation occurs. Dashed arrows represent fluxes that are only included in the climate change scenarios, dashed boxes fall outside the model domain. See text for complete discussion.

After entering the WMS through the Strait of Gibraltar, WMSW travels along the African coast and, in part, flows into the EMS via the Strait of Sicily, while the other part flows into the Tyrrhenian Sea [Schroeder *et al.*, 2008c]. Upon flowing into the EMS, SW continues traveling eastward while evaporation increases salinity. Ultimately, EMSW sinks to form EMIW that, in turn, exits the EMS through the Strait of Sicily to the WMS, and through the Strait of Otranto and the Cretan Straits to the Adriatic and Aegean Seas, respectively. Deep water formation in the Adriatic and Aegean Seas returns modified EMIW to the EMDW reservoir at a combined rate of 0.36 Sv [Van Cappellen *et al.*, 2014]. Note that the Adriatic and Aegean Seas fall outside the model domain, hence allowing us to impose DW formation as an external forcing to the THC of the EMS. To maintain the water balance of the MS, EMDW formation is offset by upwelling of EMDW into EMIW.

Deep water in the WMS forms primarily in the northwestern Mediterranean Sea (NWM). Similar to the EMS, we exclude the area of DW formation in the NWM from the model domain. The corresponding area is estimated to cover about $25^{\circ}000 \text{ km}^2$ [L'Hévéder *et al.*, 2013]. Two mechanisms contribute to DW formation in the NWM: open ocean convection and cascading of shelf water from the Gulf of Lions. Annual WMDW formation from open ocean convection in the NWM for the period 1959–2001 ranges between 0 and 3.2 Sv [L'Hévéder *et al.*, 2013] (Table S1), depending on the severity of the preceding winter. From the 1959–2001 record, we estimate a long-term annual average rate of DW formation by open ocean convection of 0.60 Sv.

Dense water cascading downslope from the Gulf of Lions also occasionally contributes to DW formation. Over a 28 day period in 1999, 0.18 Sv of water flowed down from the Gulf of Lions shelf into the WMDW reservoir [Béthoux *et al.*, 2002]. Assuming this was the only event occurring that year, an equivalent annual average rate of WMDW formation of 0.01 Sv is obtained, which is the value used in the water cycle model.

Note, however, that WMDW formation through this mechanism may be as high as 0.07 Sv (or 6% of the open ocean convection DW flux), as occurred during the extreme winters of 2005 and 2012 [*de Madron et al.*, 2005; *Ulses et al.*, 2008; *de Madron et al.*, 2013]. Using the lower value of 0.01 Sv is reasonable given that cascading of deep water only occurred in 4 years during the 1971–2000 period [*Béthoux et al.*, 2002]. In the baseline simulations, the total WMDW formation rate originating from the NWM area is thus 0.61 Sv, nearly twice the DW formation rate in the EMS (Figure 1). Deep water convection arises from preconditioning of WMSW by cyclonic circulation and Mistral wind activity, plus admixing of high-salinity WMIW which further increases water density [*Medoc Group*, 1970]. *Rhein* [1995] estimates that 38% of WMDW formation originates from WMSW and 62% from WMIW, based on chlorofluoromethane distributions. Here we assign the same proportions to the WMDW formation flux, yielding 0.23 Sv of WMDW produced from WMSW and 0.38 Sv from WMIW.

In addition to DW formation in the NWM, Tyrrhenian Deep Water (TDW) is formed in the Tyrrhenian Sea through cascading and mixing of EMIW after it enters the WMS through the Strait of Sicily [*Gasparini et al.*, 2005]. As the inflowing EMIW water is much denser than surface and intermediate waters of the Tyrrhenian Sea, it cascades down to depths of up to 2000 m. The formation of TDW is represented in the water cycle model as a conversion of WMIW into WMDW. Based on the flows of WMDW entering and exiting the Tyrrhenian Sea reported by *Schroeder et al.* [2008c], we estimate that TDW contributes 0.07 Sv to the DW reservoir of the WMS.

The upwelling fluxes from WMDW to WMIW and from WMIW to WMSW are derived assuming a steady state water cycle for the WMS. The net upwelling from WMIW to WMSW is the result of the lower water fluxes through the Strait of Gibraltar compared to the Strait of Sicily. Nonetheless, downwelling from WMSW to WMIW occasionally occurs [*Millot*, 1999; *Fuda et al.*, 2000; *Vargas-Yáñez et al.*, 2012]. Because of the lack of quantitative information on the downwelling flux, it is not included explicitly in the water cycle model.

The water cycle illustrated in Figure 1 yields a WMDW residence time of 42 years, 3 times shorter than for the EMDW (150 years). The large difference in DW residence time between the two basins of the MS is due to more intense DW formation in the WMS plus the smaller WMDW reservoir size. The residence times for surface water (SW) and IW are similarly smaller for the WMS than EMS. The WMDW residence time in the water cycle model is at the upper end of the 20–40 year range reported in older studies [*Rhein*, 1995; *Stratford et al.*, 1998; *Béthoux and Gentili*, 1999], and somewhat lower than the recently proposed 50–70 year range of *Schneider et al.* [2014], who derived mean water ages in the WMS from CFC-12 distributions.

2.2. Oxygen Cycle

The O₂ mass balance model explicitly computes O₂ reservoir sizes of the IW and DW layers. Oxygen in SW is assumed to remain near saturation with the atmosphere so is not explicitly modeled. The model is initialized by assigning average O₂ concentrations to the SW, IW, and DW layers obtained from the MEDATLAS database for the period 1906–1987 [*MEDAR Group*, 2002] (Figures 2 and S1 and Table S2). For comparison, oxygen concentrations reported for individual cruises are compiled in Table S2. With the exception of the turbulent mixing exchanges, O₂ fluxes between reservoirs are computed by multiplying the corresponding water flow with the O₂ concentration of the source reservoir. For the water supplied to the WMDW reservoir from the NWM DW formation area, the O₂ concentration is assumed to be that of the WMSW, because of the intense mixing that occurs during deep convection [*Medoc Group*, 1970]. For DW formation in the EMS, we impose average winter O₂ concentrations measured in the deeper (>800 m) waters of the Adriatic and Aegean Seas because these water masses are the source areas of the newly formed DW entering the EMDW through the Strait of Otranto and Cretan Straits, respectively (Table S2).

Van Cappellen et al. [2014] modeled the turbulent mixing fluxes of P and N between EMSW and EMIW assuming a linear dependence on the concentration differences between the two water masses, with an effective diffusion coefficient K_z of $2.3 \times 10^{-4} \text{ m}^2 \text{ s}^{-1}$. Because turbulent mixing is somewhat weaker in the WMS [*Moutin and Raimbault*, 2002], a comparable, but smaller K_z value ($1.2 \times 10^{-4} \text{ m}^2 \text{ s}^{-1}$) is used to calculate mixing fluxes of O₂ between WMSW and WMIW. *Cuypers et al.* [2012] further showed that very little mixing occurs between IW and DW water layers. Therefore, we impose a low K_z value of $10^{-7} \text{ m}^2 \text{ s}^{-1}$ for turbulent diffusion of O₂ between WMIW and WMDW, and between EMIW and EMDW. This value falls at the lower end of the reported range of measured K_z values in the MS (10^{-7} to $7 \times 10^{-4} \text{ m}^2 \text{ s}^{-1}$) [*Bianchi et al.*, 1999; *Copin-Montégut*, 2000; *Moutin and Raimbault*, 2002; *Cuypers et al.*, 2012; *Forryan et al.*, 2012].

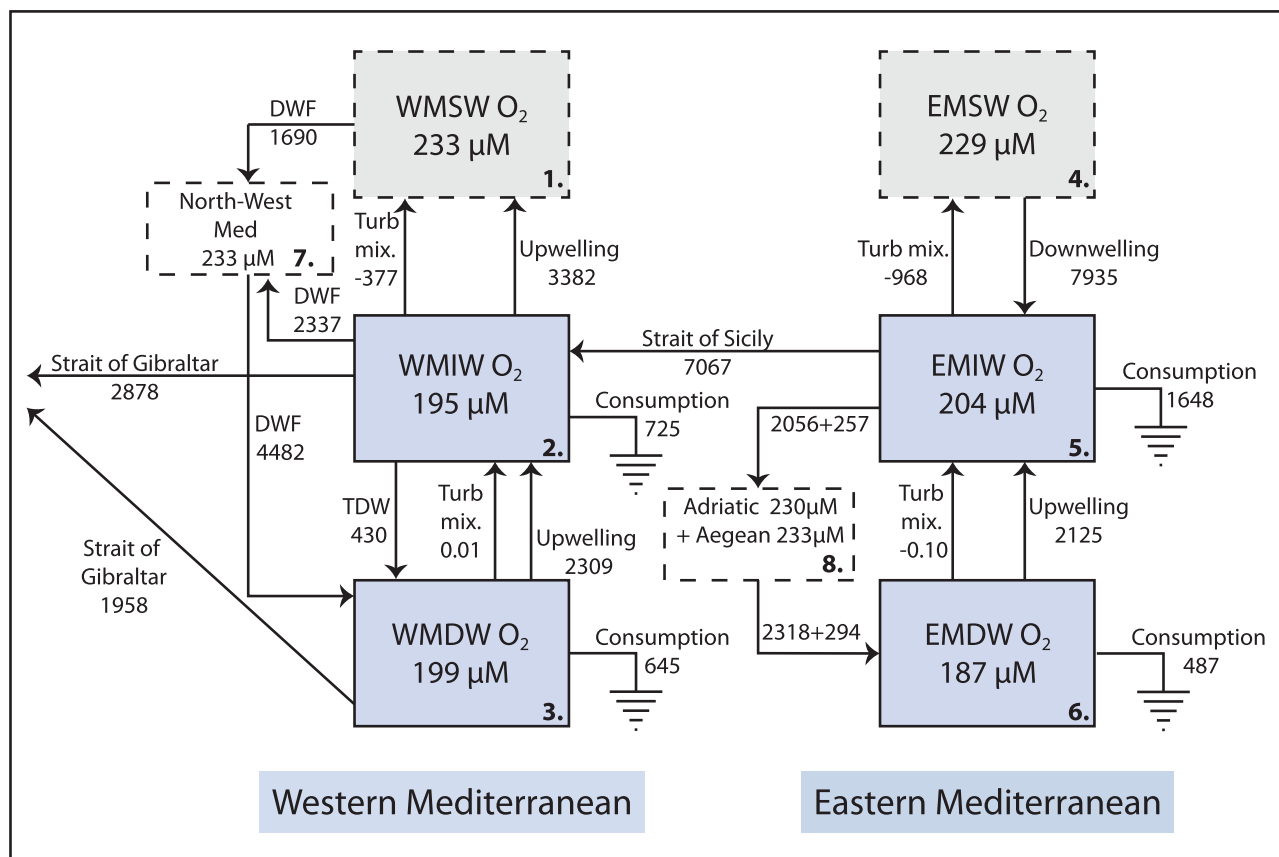


Figure 2. Baseline (pre-EMT) steady state oxygen cycle. Dashed boxes represent reservoirs outside the model domain. Fluxes are given in 10^9 mol yr^{-1} . DWF = deep water formation; TDW = Tyrrhenian deep water formation. See text for complete discussion.

Once the O_2 fluxes between reservoirs are known, the pre-EMT O_2 consumption rates are obtained assuming a steady state O_2 cycle (Figure 2). In order to model transient changes in O_2 cycling, two formulations for the O_2 consumption rate are considered. In the first formulation, a simple kinetic expression is used

$$F_{\text{O}_2,i} = F_{\text{max},i} \cdot \frac{[\text{O}_2]_i}{[\text{O}_2]_i + K_s}, \quad i = \text{WMIW, WMDW, EMIW, EMDW}, \quad (1)$$

where F_{O_2} is the annual O_2 consumption rate in a given water layer (in mol yr^{-1}), F_{max} is the maximum (or potential) O_2 consumption rate in the same water layer, when O_2 is nonlimiting, $[\text{O}_2]$ is the O_2 concentration of the water layer (μM), and K_s is the O_2 half-saturation concentration, which is assigned the value of $6.25 \mu\text{M}$ proposed by Testa *et al.* [2014]. For each of the IW plus DW reservoirs the value of F_{max} is calculated from the corresponding pre-EMT steady state O_2 concentration and consumption rate (Table S3).

Equation (1) is based on the classical Michaelis-Menten saturation formulation for the biological utilization of a substrate. When the O_2 concentration significantly exceeds the half saturation value K_s , the O_2 consumption rate is independent of $[\text{O}_2]$ and approaches its maximum value F_{max} . This is the case for the present-day open MS for which $[\text{O}_2] \gg K_s$ at all depths. The use of equation (1) assumes that the reducing power available for O_2 respiration in a given water layer does not change over time. The main source of reducing power is the supply of degradable organic matter, either as POC associated with sinking particulate matter or DOC present in inflowing water.

Marked increases in DW O_2 consumption during the EMT and WMT have been attributed to the enhanced supply of (relatively) labile DOC originating from the areas of DW formation [Klein *et al.*, 2003; Schneider *et al.*, 2014]. The second formulation for the oxygen consumption rate in the DW reservoirs therefore expands equation (1) in order to account for both the relatively fast respiration of labile DOC, supplied from the Adriatic, Aegean and NWM, and the slower degradation of sinking POC

$$F_{O_2,i} = \left(F_{max,i}^{DOC} \cdot \frac{[DOC]_i}{[DOC]_i + K_{DOC}} + F_{max,i}^{POC} \right) \cdot \frac{[O_2]_i}{[O_2]_i + K_s}, \quad i = \text{WMDW, EMDW}, \quad (2)$$

where F_{max}^{DOC} and F_{max}^{POC} are the maximum DW O_2 consumption rates associated with DOC and POC respiration, respectively, $[DOC]$ is the DOC concentration in the DW reservoir, and K_{DOC} is the DOC half-saturation concentration, which is assigned the value of 4.16 μM proposed by *Testa et al.* [2014]. As written, equation (2) requires the explicit calculation of the changes in DW DOC concentrations. To circumvent this requirement, we replace $[DOC]$ in equation (2) by the (virtual) DOC-associated O_2 concentration, that is, the portion of the total O_2 concentration in the DW reservoir that can react with DOC. To use the modified equation (2), values must be assigned to F_{max}^{POC} and F_{max}^{DOC} , as well as to the initial DOC-associated O_2 concentration of the DW reservoir. The DOC half-saturation concentration K_{DOC} is converted into an O_2 half saturation concentration using a molar O_2 :C ratio of 172:122 [*Takahashi et al.*, 1985].

For the EMS, F_{max}^{POC} is estimated based on the EMDW O_2 consumption rates before and during the EMT. The pre-EMT O_2 consumption rate is that derived for the steady state O_2 cycle ($487 \times 10^9 \text{ mol yr}^{-1}$ or $0.29 \mu\text{M yr}^{-1}$, Figure 2). For the EMT, the rate is approximated by considering the observed O_2 consumption in Aegean DW ($2.3 \mu\text{mol kg}^{-1} \text{ yr}^{-1}$) [*Klein et al.*, 2003] and the total volume of Aegean DW that entered the EMDW reservoir during the EMT, that is, between 1987 and 1995 ($2.3 \times 10^{14} \text{ m}^3$) [*Roether et al.*, 2007]. Assigning the pre-EMT O_2 consumption rate ($0.29 \mu\text{M yr}^{-1}$) to the volume of EMDW not replaced by inflowing Aegean DW over the same period of time then yields an average annual O_2 consumption rate for the entire EMDW during the EMT of $965 \times 10^9 \text{ mol yr}^{-1}$ (or $0.57 \mu\text{M yr}^{-1}$). If we further assume a linear dependence of the rate of EMDW O_2 consumption on the rate of DW formation (Figure S2), a value of F_{max}^{POC} of $295 \times 10^9 \text{ mol yr}^{-1}$ is derived from the y intercept of the linear relationship. We are now left with two unknowns, F_{max}^{DOC} and the DOC-associated O_2 concentration. These two variables are coupled to one another via equation (2) under the steady state, pre-EMT conditions. Next, the initial DOC-associated O_2 concentration is varied until the predicted temporal trend of the EMDW O_2 concentration satisfactorily reproduces the observed O_2 variations during the EMT (see section 4.2).

For the WMS, *Christensen et al.* [1989] estimate that before the WMT, 22% of O_2 respiration in the WMDW was associated with the flux of sinking POC and 78% with the mineralization of inflowing DOC. If for the WMS we assume the same maximum DOC-associated O_2 consumption rate per unit volume of water as for the EMS, then the initial DOC-associated O_2 concentration in WMDW can be calculated directly from the pre-WMT steady state O_2 consumption rate. With all parameter values in equation (2) known, the fractions of DOC-associated O_2 in water flows supplied to the WMDW and EMDW can be calculated from the condition of steady state. Maximum (potential) O_2 consumption rates used in equation (2) for the WMS and EMS are summarized in Table S4.

2.3. Numerical Solution and Factorial Design Analysis

The ordinary differential equations describing the O_2 mass balances of the two IW and two DW reservoirs are solved in MATLAB using ODE solver 15s. A 2^{25-15} fractional factorial design analysis [*Box et al.*, 1978; *Van Cappellen et al.*, 2014] of the model with equation (1) is used to assess the sensitivity of O_2 concentrations in the IW and DW reservoirs to model parameters. A factorial design analysis measures the sensitivity of a given model response (here the IW and DW O_2 concentrations) to each individual model parameter, as well as to interactions between model parameters. Here we only consider first (one parameter) and second-order (two parameter) interactions as the fairly simple model dynamics are largely insensitive to higher-order parameter interactions [*Van Cappellen et al.*, 2014]. Parameters included in the analysis are the SW O_2 concentration of the EMS and WMS, the O_2 concentration of inflowing DW from the Adriatic and Aegean Seas, the values of F_{max} , K_s , and K_z , plus all water fluxes in the water cycle. All model parameters are varied by $\pm 10\%$, and the effects on the model responses are calculated using Yate's algorithm [*Box et al.*, 1978]. The results of the factorial design analysis are plotted on a probability versus effect graph for each of the four model responses (the O_2 concentrations of WMIW, WMDW, EMIW, and EMDW; Figure S3): parameters that yield responses along the vertical line centered on the origin are considered insensitive, the further a response deviates from the vertical line, the more sensitive the corresponding parameter.

Table 1. Water Fluxes Assigned to Pre-EMT (Before 1987), EMT, WMT, and the Three Climate Change Scenarios (WC1–WC3)^a

	Climate Change Scenarios							
	EMT				WMT	WC1	WC2	WC3
	Pre-EMT	1987–1992	1992–1994	1994–2002	2004–2006	Weaker THC	Weaker in WMS, Stronger in EMS	Stronger THC
<i>WMS</i>								
Net evaporation (F_{1E})	0.01	0.01	0.01	0.01	0.01	0.01	0.01	0.01
Atlantic SW (F_{G1})	0.83	0.83	0.83	0.83	0.83	0.83	0.84	0.83
IW-Atl (F_{2G})	0.47	0.47	0.47	0.47	0.27	0.51	0.47	0.40
DW-Atl (F_{3G})	0.31	0.31	0.31	0.31	0.52	0.24	0.29	0.36
IW-SW (F_{21})	0.55	0.55	0.55	0.55	1.22	0.04	0.73	0.84
SW-NWM (F_{17})	0.23	0.23	0.23	0.23	0.90	0.18	0.19	0.40
IW-NWM (F_{27})	0.38	0.38	0.38	0.38	1.50	0.30	0.31	0.66
NWM-IW (F_{72})	0	0	0	0	0	0.33	0	0
NWM-DW (F_{73})	0.61	0.61	0.61	0.61	2.40	0.16	0.50	1.06
IW-DW (F_{23})	0.07	0.07	0.07	0.07	0.07	0.09	0.06	0.12
DW-IW (F_{32})	0.37	0.37	0.37	0.37	1.95	0	0.27	0.82
<i>Strait of Sicily</i>								
WMS-EMS SW (F_{14})	1.14	1.14	1.14	1.14	1.14	0.67	1.37	1.26
EMS-WMS IW (F_{52})	1.10	1.10	1.10	1.10	1.10	0.61	1.30	1.20
<i>EMS</i>								
Net evaporation (F_{4E})	0.06	0.06	0.06	0.06	0.06	0.07	0.08	0.07
Adr+Aeg to SW (F_{84})	0.02	0.02	0.02	0.02	0.02	0	0.01	0.01
SW-IW (F_{45})	1.10	1.10	1.10	1.10	1.10	0.61	1.30	1.20
IW to Adri+Aeg (F_{58})	0.36	0.38	3.02	0.57	0.36	0.47	2.35	2.30
Adr+Aeg to IW (F_{85})	0	0	0	0	0	0.42	0	0
Adri+Aeg to DW (F_{86})	0.36	0.38	3.02	0.57	0.36	0.05	2.35	2.30
DW-IW (F_{65})	0.36	0.38	3.02	0.57	0.36	0.05	2.35	2.30

^aNumbering of fluxes is that of Figure 1. Atl = Atlantic, NWM = North-West Mediterranean, Adri = Adriatic, Aeg = Aegean, Net evaporation = evaporation – river discharge – submarine groundwater discharge. Units: Sv ($10^6 \text{ m}^3 \text{ s}^{-1}$).

3. Scenarios

3.1. Recent Changes: EMT and WMT

The EMT and WMT are simulated using the changes in water fluxes summarized in Table 1. For the EMS, these changes are the same as those imposed by Powley *et al.* [2014] who assessed the EMT impacts on the cycling of P and N in the EMS. The main EMT pulse occurred between 1992 and 1994 during which Aegean DW formation increased by almost 2 orders of magnitude relative to that prior to the EMT [Roether *et al.*, 2007]. After 2002, circulation in the EMS is assumed to return to pre-EMT conditions.

The WMDW formation rate during the 2004–2006 WMT is estimated at 2.4 Sv, that is, 4 times the pre-WMT average. The upwelling fluxes in the WMS (F_{21} and F_{32} in Figure 1) are adjusted to balance the higher DW formation rate during the WMT. This is consistent with observations: by October 2006, less than 2 years after the WMT started, the newly formed WMDW had spread across most of the WMS, with the exception of the Tyrrhenian Sea and the western part of the Alboran Sea [Schroeder *et al.*, 2008b]. Variations in the WMDW formation rate also affect the mix of WMDW and WMIW exiting the WMS through the Strait of Gibraltar [García Lafuente *et al.*, 2007]. On an annual basis, about 10% of the total outflow through the Strait of Gibraltar is generated by seasonal DW formation, while 30% is uncoupled from the seasonal signal [García Lafuente *et al.*, 2007]. Presumably, the latter 30% correspond to the WMDW outflow driven by Bernoulli suction resulting from the fast current speeds through the Strait. Assuming that the yearly outflow of WMDW by Bernoulli suction remains fixed at 30%, increased WMDW formation during the WMT raised the contribution of WMDW from 40 to 66% while, simultaneously, the contribution of WMIW dropped from 60 to 34%.

The changes in O_2 concentrations accompanying the EMT and WMT are assessed using either equation (1) for all four IW and DW reservoirs, or equation (1) for the IW reservoirs and equation (2) for the DW reservoirs. In the first case, potential O_2 consumption rates of each reservoir remain unchanged (i.e., F_{max} is constant). In the second case, the potential O_2 consumption rate coupled to the oxidation of sinking POC remains constant (i.e., F_{max}^{POC} is constant). For the DW reservoirs, however, the O_2 consumption rate associated with the

Table 2. Climate Change Scenarios

Scenario	Description
Sol	Solubility: Decrease SW solubility by 2.8 and 6.3%, use equation (1)
Kin	Kinetics: Increase F_{max} by 7.8 and 14.9% in IW, and 4.8 and 10.0% in DW, use equation (1)
WC1.1	Water circulation scenario 1 with equation (1) for deep water oxygen consumption plus scenarios Sol and Kin . <i>THC:</i> 75% decrease in WMDW production, 85% decrease in EMDW production, 45% decrease in EMIW to WMIW based on <i>Somot et al.</i> [2006]
WC1.2	Water circulation scenario 1 with equation (2) (see section 3.2 for details) plus scenarios Sol and Kin
WC2.1	Water circulation scenario 2 with equation (1) plus scenarios Sol and Kin . <i>THC:</i> 18% decrease in WMDW production, 553% increase in EMDW production, 18% increase in EMIW to WMIW, based on A2-ARF: <i>Adloff et al.</i> [2015]
WC2.2	Water circulation scenario 2 with equation (2) plus scenarios Sol and Kin
WC3.1	Water circulation scenario 3 with equation (1) plus scenarios Sol and Kin . <i>THC:</i> 73% increase in WMDW production, 539% increase in EMDW formation, 9% increase in EMIW to WMIW, based on B1-ARF: <i>Adloff et al.</i> [2015]
WC3.2	Water circulation scenario 3 with equation (2) plus scenarios Sol and Kin

oxidation of labile DOC responds to changes in DW formation, because of the corresponding variations in the DOC input to the DW reservoir.

3.2. Future Changes: Climate Change Perturbations

Adloff et al. [2015] estimate that by 2100 climate change will raise temperatures and salinities in the top 150 m of the MS between 1.29 and 2.30°C and between 0.58 and 0.74, respectively, altering O₂ solubility of SW (Scenario Sol). Increased water temperatures may also increase the rate of organic matter degradation and thus oxygen consumption [*Brewer and Peltzer*, 2016]. The temperature effect on the O₂ consumption kinetics (Scenario Kin) are simulated using equation (1) and assuming a Q₁₀ value of 2 [*Vichi et al.*, 2015], together with predicted 2100 temperature increases for IW (1.26–2.0°C) and DW (0.68–1.38°C) [*Adloff et al.*, 2015]. Details on the implementation of the scenarios are given in Table 2. Note that spatial differences in temperature and salinity changes between the EMS and WMS are ignored. As shown below, this does not affect the main conclusions.

Three different scenarios (WC1, WC2, and WC3) cover the range of projected changes in Mediterranean THC by the year 2100. The first scenario (WC1) is based on the work of *Somot et al.* [2006], who predict a weakening of THC in both the WMS and EMS. Scenarios WC2 and WC3 are based on the results of the A2-ARF and B1-ARF scenarios of *Adloff et al.* [2015], respectively. In WC2 THC becomes weaker in the WMS, but strengthens in the EMS, while in WC3 THC is more vigorous in both the WMS and EMS. The corresponding changes in the water fluxes are summarized in Table 1. For each scenario, a stepwise change to the pre-EMT water cycle is imposed and the O₂ mass balance model is run until a new steady state is reached. For the DW reservoirs, either equation (1) or equation (2) is used to calculate O₂ consumption (see Table 2). Each circulation scenario is combined with the maximum and minimum changes in SW O₂ solubility and O₂ consumption kinetics.

In WC1, WMDW formation decreases by 74% and that of EMDW by 85%, relative to the baseline values. These changes are attributed to temperature-driven density changes and a decrease in wind stress at the DW formation sites [*Somot et al.*, 2006], both important factors in the preconditioning of water prior to DW formation. The volume of water flowing over the Otranto shelf out of the Adriatic Sea, however, increases by 37% compared to pre-EMT circulation. This water, however, does not cascade deeper than 1000 m [*Somot et al.*, 2006]. In WC1, excess water exiting the Adriatic and Aegean Seas that does not become EMDW is therefore redirected into the EMIW reservoir, which requires adding an additional water flow in the water cycle (F_{85} in Figure 1). Similarly, for the WMS the additional flow F_{72} accounts for the shallower penetration of DW formation originating in the NWM as a result of climate warming, as also proposed by *Herrmann et al.* [2008].

Somot et al. [2006] further predict a 45% decrease in the westward flow of EMIW between the Ionian and Levantine basins. In WC1, we assume that this decrease in flow propagates to the Strait of Sicily, that is, we impose a 45% drop in the EMIW outflow to the WMS. To maintain water balance, the model then requires a 45% decrease in EMIW formation. In addition, cessation of surface flow from the Adriatic and Aegean Seas into the EMS occurs because, under the projected climate conditions, both basins transition from net dilution (E-R-P < 0) to net concentration (E-P-R > 0) [*Somot et al.*, 2006]. The projected circulation changes of

Somot et al. [2006] also predict a small, 4% decline in the outflow from the WMS to the Atlantic Ocean, while the decreased WMDW formation implies a smaller contribution of WMDW to the outflow across the Strait of Gibraltar: 33% in WC1, compared to 40% in the baseline water cycle.

In WC2, an EMT-like circulation regime is simulated, based on the A2-ARF scenario of *Adloff et al.* [2015]. The imposed 18% decrease in WMDW formation assumes that the relative change in DW formation is proportional to the change in mixed layer depth of the NWM in the A2-ARF scenario. The 2.2 Sv DW formation from the Aegean Sea is derived from the EMT index, which compares the maximum zonal overturning function in the deep Ionian Basin to the minimum value in the Levantine Basin [*Adloff et al.*, 2015]. Adriatic DW formation is estimated at 0.15 Sv based on the meridional overturning function at the Strait of Otranto. The flux of water through the Strait of Sicily is estimated to increase by 0.2 Sv [*Adloff et al.*, 2015], while evaporation over the entire MS increases by 52%.

In WC3, SW density increases throughout the MS, leading to a strengthening of the THC in both EMS and WMS. The same method as in WC2 is applied to derive fluxes from the results of the B2-ARF scenario reported by *Adloff et al.* [2015]. A 73% increase in DW formation over the Gulf of Lions is estimated, while the contribution of Aegean DW formation is slightly weaker at 2.0 Sv, with the Adriatic contributing 0.3 Sv. The water balance then requires a 0.1 Sv increase in the flux of water through the Strait of Sicily.

4. Results and Discussion

The expansion of bottom water hypoxia in marine environments as a result of global warming is a growing concern [*Rabalais et al.*, 2010; *Doney et al.*, 2012; *Altieri and Gedan*, 2015]. The potential for O₂ depletion is particularly high in shallow coastal environments, and in marginal or semienclosed marine basins such as the Bohai, Baltic, and Mediterranean Seas [*Zhai et al.*, 2012; *Carstensen et al.*, 2014; *Friedrich et al.*, 2014]. The Mediterranean sedimentary record further shows that during the recent geological past, the EMS experienced repeated periods of basin-wide hypoxia characterized by the deposition of sapropels [*Rohling et al.*, 2015, and references therein]. Thus, with the MS region expected to undergo some of the world's fastest warming in the coming decades [*Giorgi*, 2006], the sensitivity of deep water oxygenation to climate change deserves particular attention. Our approach is based on simple mass balance calculations of the water and dissolved O₂ cycles in the MS. The approach does not resolve the spatial and intra annual variability in circulation and oxygen consumption across the MS basin. Rather the approach is designed to interrogate the key dynamic couplings between circulation and the biogeochemical functioning of the MS system on a yearly averaged, basin-wide scale [i.e., *Béthoux et al.*, 1992; *Powley et al.*, 2014; *Van Cappellen et al.*, 2014].

4.1. Baseline O₂ Cycling (Pre-EMT)

The factorial design analysis indicates that O₂ concentrations in WMIW and EMIW are highly sensitive to the imposed SW O₂ concentrations (Figures S3A and S3B). Interestingly, the WMIW O₂ concentration is more sensitive to the SW O₂ concentration of the EMS than that of the WMS (Figure S3A). This is a direct consequence of the water cycle model in which the majority of WMIW is produced by inflow of EMIW, thus highlighting the closely intertwined O₂ dynamics of the two Mediterranean basins. Not surprisingly, deep water O₂ concentrations in both the WMS and EMS are sensitive to the water flows in and out of the DW reservoirs, as well as the O₂ concentrations in the water reservoirs where DW formation originates (Figures S3C and S3D). In addition, the O₂ concentrations in all IW and DW reservoirs are sensitive to the maximum potential rates of O₂ consumption.

Per unit volume, the baseline O₂ consumption rates are greater in WMDW than in EMDW, but lower in WMIW than EMIW despite the higher primary productivity in the WMS compared with the EMS [*Antoine et al.*, 1995]. A higher influx of labile and semilabile DOC into the WMDW [*Santinelli*, 2015], which enhances heterotrophic respiration in the DWs of the WMS [*Luna et al.*, 2012], helps explain the 2.5 times larger O₂ consumption rate in WMDW (0.71 μM yr⁻¹; Table S5) compared to EMDW (0.29 μM yr⁻¹; Table S5). The two-fold difference in O₂ consumption rate between EMIW (4.12 μM yr⁻¹) and WMIW (2.23 μM yr⁻¹) is similarly attributed to differences in the input of degradable DOC. Downwelling in the eastern part of the EMS supplies relatively labile DOC from the euphotic zone to the EMIW. However, by the time the EMIW exits the EMS through the Strait of Sicily, the remaining DOC supplied to the WMIW is more refractory than that in the EMIW. Upwelling of WMDW into WMIW likely also delivers relatively refractory DOC. Thus, the lower O₂

respiration rates in WMIW compared to EMIW are primarily the result of differences in the supply of DOC, rather than that of POC, which is actually 1.8 times greater per unit surface area in the WMS than EMS [Moutin and Raimbault, 2002].

The predicted baseline O₂ consumption rates generally agree with literature estimates for the period prior to the EMT (1987) for the EMS, and prior to the WMT (2004) for the WMS. For example, electron transport system (ETS) activity measurements by Christensen *et al.* [1989] in the WMS yield an equivalent O₂ respiration rate for the 500–3500 m depth range on the order of 0.6 μM O₂ yr⁻¹, which is close to the value of 0.71 μM O₂ yr⁻¹ we derive for the WMDW. Similarly, our modeled WMIW rate of 2.2 μM O₂ yr⁻¹ falls in the range for the 110–1000 m depth interval (1.4–5.5 μM O₂ yr⁻¹) inferred from ETS activity measurements [Savenkoff *et al.*, 1993; Lefèvre *et al.*, 1996; Tanaka and Rassoulzadegan, 2004]. Using a mass balance approach, Roether and Well [2001] derived an O₂ consumption rate of 0.55 μM O₂ yr⁻¹ for the EMS below 1000 m, compared to our EMDW value of 0.29 μM O₂ yr⁻¹. We are not aware of independent O₂ consumption rate determinations for the EMIW prior to the onset of the EMT.

The O₂ consumption rates in WMDW and EMDW are higher than the average respiration rate of 0.13 ± 0.03 μM O₂ yr⁻¹ reported by Williams [2014] for the bathypelagic depth range (1000–4000 m) of the global ocean. In contrast, O₂ consumption rates in WMIW and EMIW are lower than the global average mesopelagic (150–1000 m) value of 4.18 ± 0.68 μM O₂ yr⁻¹ [Williams, 2014]. Our analysis suggests that the anomalous depth distribution of O₂ consumption rates of the MS reflects the important contribution to DW respiration of labile and semilabile DOC supplied from the SW source areas of deep water formation. However, the relatively high DW temperatures of the MS may also in part explain why the DW O₂ consumption rates exceed the world ocean average value [Roether and Well, 2001].

4.2. EMT-WMT

The responses of the DW and IW O₂ concentrations to the well-documented, large-scale changes in THC known as EMT and WMT provide an opportunity to test the coupled water-O₂ cycle model. Overall, modeled O₂ concentrations of EMIW and EMDW are quite sensitive to the EMT (Figure 3A). Use of both equations (1) and (2) captures the approximately 5 μM increase in EMDW O₂ concentration measured immediately following the main EMT pulse [Klein *et al.*, 2003; Kress *et al.*, 2003]. However, with equation (1), the model predicts a further increase in EMDW O₂ concentration until at least the turn of the century, contrary to the reported decrease after 1995 [Klein *et al.*, 2003]. In contrast, equation (2) predicts a decrease of post-1995 EMDW O₂ concentrations. The trend in EMDW O₂ consumption predicted using equation (2) reflects the decomposition of the relatively labile DOC accompanying the pulse of enhanced Aegean DW formation during the EMT.

The modeled EMIW O₂ concentration shows an opposite trend to that of EMDW, with a decrease between 1987 and 1995 followed by a recovery to pre-EMT values (Figure 3A). Equations (1) and (2) yield nearly identical temporal trends for the EMIW O₂ concentration. The initial model-derived drop of about 4 μM is lower than some observed reductions in EMIW O₂ concentration caused by the EMT. For instance, within the Levantine Basin the IW O₂ concentration dropped by as much as 40 μM between 1987 and 1999 [Kress *et al.*, 2003]. During that period, however, a blocking anticyclone stopped the eastward flow of SW into the Levantine Basin [Kress *et al.*, 2003], hence regionally increasing the IW residence time and allowing for a more extensive drawdown of O₂. Similarly, in the Ionian basin, the EMT brought older, more O₂ depleted, Adriatic DW into the EMIW, causing the O₂ concentration to decrease by 15 μM [Kress *et al.*, 2003]. Our model, however, does not resolve these intrabasin mesoscale circulation features, but rather averages them out over the entire EMS. The model-predicted average EMIW O₂ consumption rate of 4.1 μM yr⁻¹ between 1999 and 2008 is of the same order of magnitude as the values of 6–8 μM O₂ yr⁻¹ derived from DOC mineralization fluxes estimated by Santinelli *et al.* [2010, 2012] for the same time period.

According to the model, between 1987 and 1999 the EMT caused a slight decrease of the WMIW O₂ concentration of about 1 μM, but it had no effect on the WMDW O₂ concentration (Figure 3B). The WMT, however, increased O₂ concentrations in both WMIW and WMDW reservoirs. This agrees with the high O₂ content reported for newly formed WMDW associated with the WMT [Schroeder *et al.*, 2008a]. With equation (1) the model predicts that, following the WMT, the WMDW O₂ concentration would remain elevated until at least 2015. Applying equation (2), however, results in a distinct drop in the WMDW O₂ concentration after 2007, which is consistent with observed WMDW O₂ concentrations in 2011 that are even lower than pre-WMT

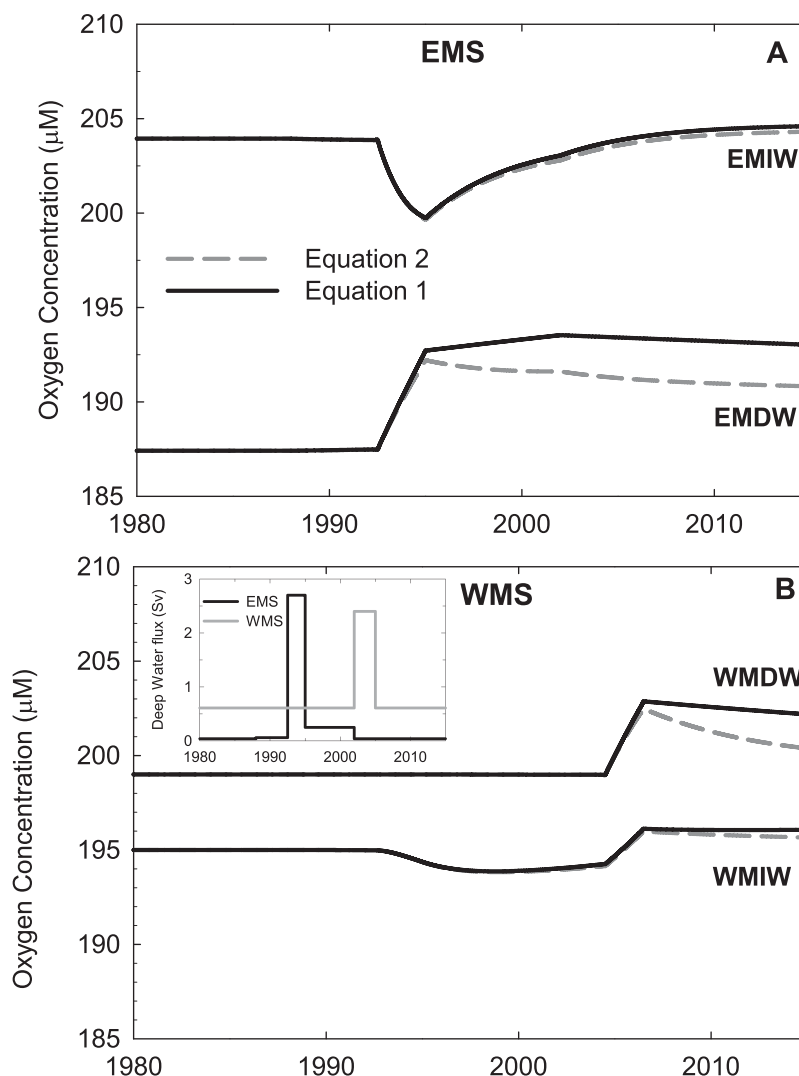


Figure 3. Response of O_2 concentrations (μM) to the EMT and WMT in (A) the EMS and (B) the WMS between 1980 and 2015 using equation (1) (black solid lines) and equation (2) (gray dashed lines) for DW O_2 consumption. Inset figure shows the time dependent changes in water influx (Sv) from the Aegean Sea (EMS, black line) and from the NWM (WMS, gray line).

values in some localities [Schneider *et al.*, 2014]. For WMIW, both equations (1) and (2) yield little change in the post-2007 O_2 concentration, in line with the lack of a systematic temporal change in measured WMIW O_2 concentrations between 2007 and 2011 [Schneider *et al.*, 2014]. Overall, equation (2), which implicitly accounts for the combined transport of SW-derived O_2 and DOC during DW formation, results in the better match to the observed, basin-scale changes in DW and IW O_2 concentrations caused by the EMT and WMT.

4.3. Sensitivity to Climate Change

Climate warming is expected to strongly impact the Mediterranean region [Giorgi, 2006; Collins *et al.*, 2013; Kirtman *et al.*, 2013]. The climate change perturbations implemented in the water- O_2 mass balance model are designed to test the sensitivity of DW and IW O_2 concentrations in the MS to potential variations in biogeochemical factors (O_2 solubility, mineralization kinetics) and THC regimes driven by the climatic conditions that are anticipated to prevail toward the end of the 21st century. Figure 4 shows the resulting changes in O_2 concentrations in each of the five climate change scenarios (Sol, Kin, WC1, WC2, and WC3).

4.3.1. Short-Term Responses (≤ 100 Years)

Luna *et al.* [2012] hypothesize that climate warming will accelerate microbial degradation of organic matter in the MS, resulting in lower water column O_2 concentrations. Scenario Kin, however, only yields very small decreases in O_2 concentrations (2–5 μM or 1–2%) for the IW and DW reservoirs in both basins of the MS

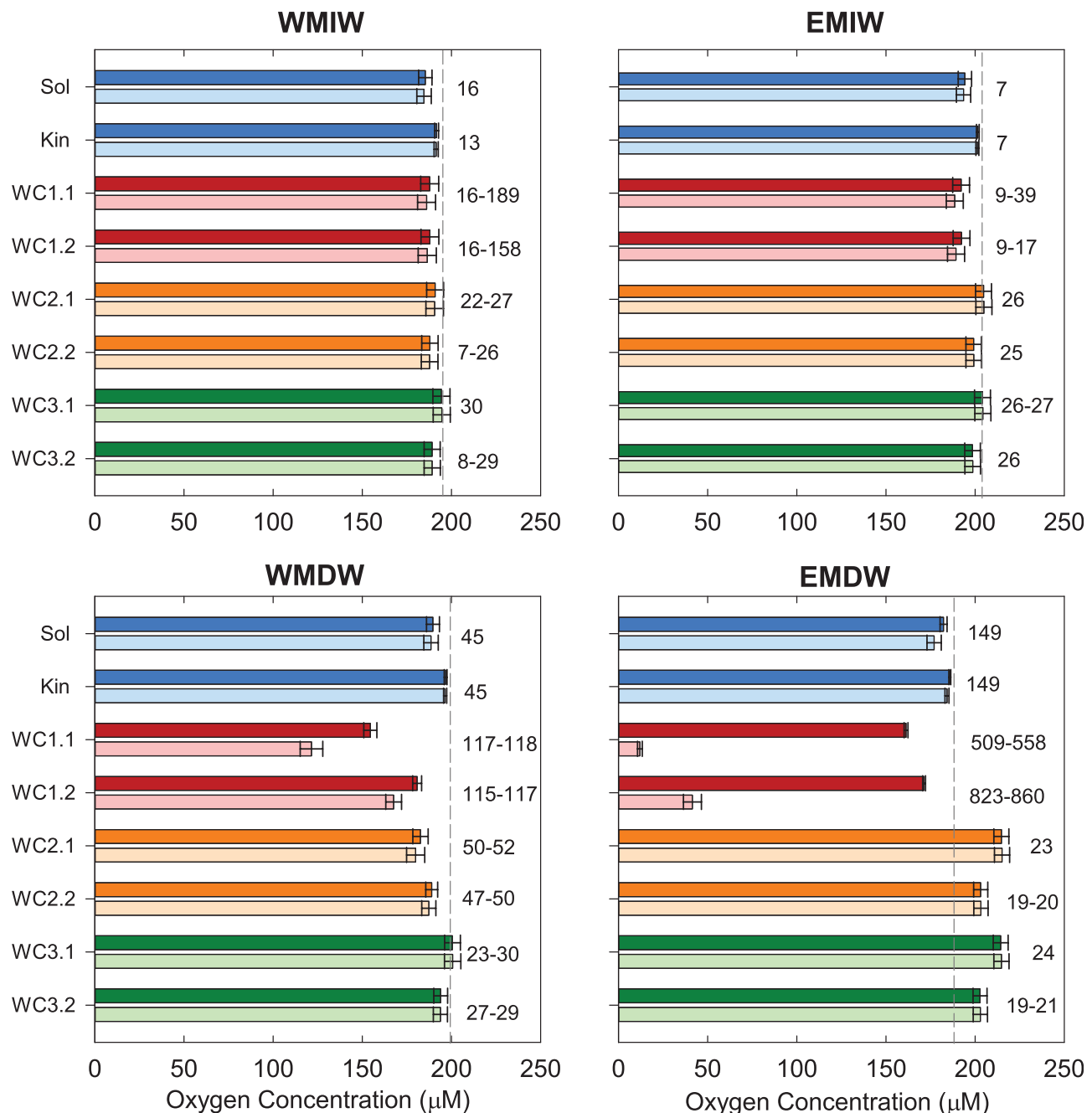


Figure 4. Intermediate and deep water O₂ concentrations of the WMS and EMS for the climate scenarios, relative to the baseline values (dashed vertical line), after 100 years (dark bars) and upon reaching steady state (light bars). Results for WC1.1, WC2.1, and WC3.1 are those obtained using equation (1) for IW and DW; results for WC1.2, WC2.2, and WC3.2 are those using equation (1) for IW and equation (2) for DW. Error bars reflect the uncertainties associated with the projected increases in water column temperatures and salinities by the year 2100. Numbers adjacent to the horizontal bars are the response times (e-folding times) to the imposed perturbations (years).

(Figure 4). Decreased SW O₂ solubility due to increased temperatures and salinity (Scenario Sol) produces somewhat larger effects on IW and DW O₂ concentrations, in line with the results of the factorial design analysis (Figure S3). After 100 years of lower SW O₂ solubilities, IW and DW O₂ concentrations in the WMS and EMS drop by 2–7% (3–13 μM), while the combined changes in solubility and kinetics produces decreases between 2 and 9% in IW and DW O₂ concentrations.

Changes in THC have the largest impacts on the O₂ concentrations of the WMDW and EMDW (Figure 4). In scenario WC1.1 the weakening of the THC causes the WMDW O₂ concentration to decrease to 151–158 μM (i.e., a 21–24% drop relative to the initial value) after 100 years, and those in the EMDW to 160–162 μM (or a

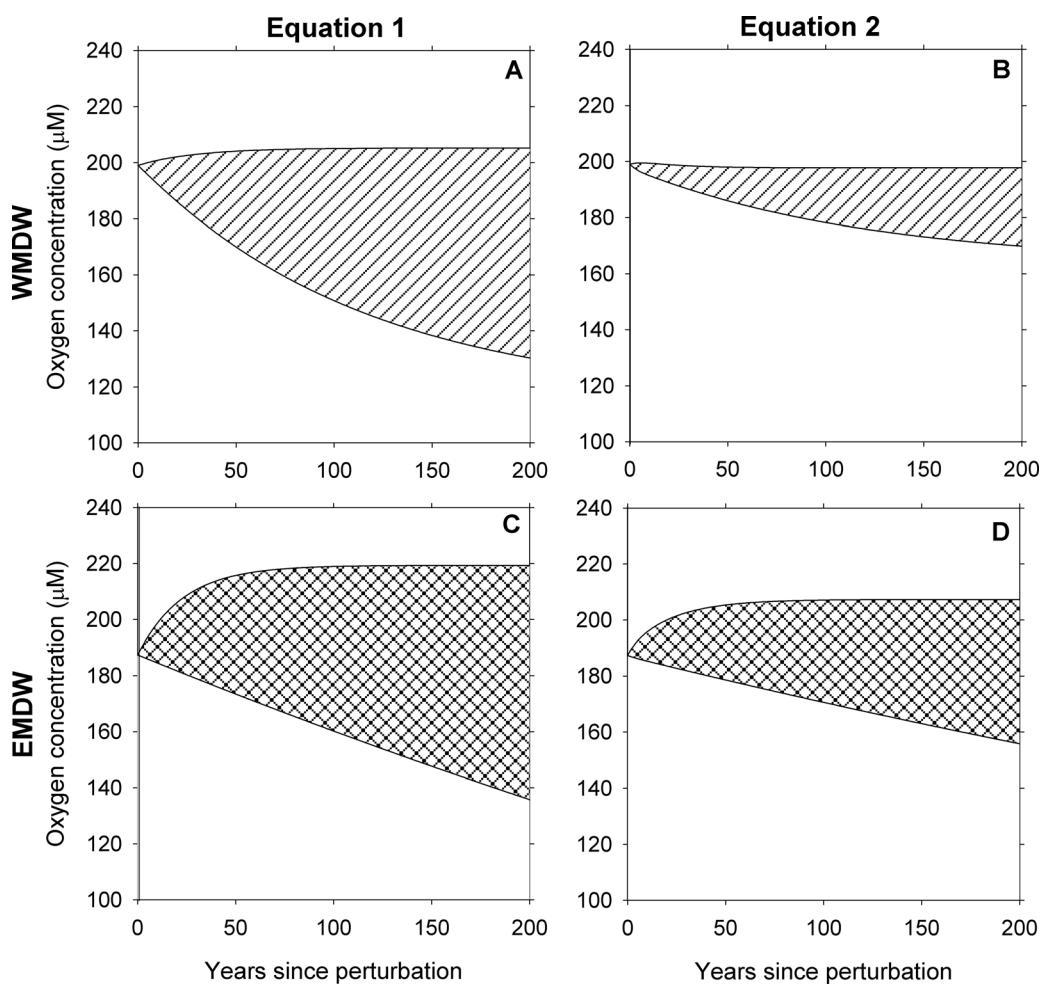


Figure 5. Ranges in simulated O_2 concentrations in WMDW (A, B) and EMDW (C, D) for 200 years after imposing the perturbations using equation (1) (A, C) and equation (2) (B, D) for the DW O_2 consumption rate. The ranges enclose the results of all the scenarios described in Table 2.

drop of 13–15%). Consequently, on a 100 year timescale WMDW appears to be more sensitive to a weakening of THC than EMDW. Climate change, however, may not necessarily result in a generalized decrease in THC across the MS. In WC2.1, where a weakening of the THC occurs in the WMS and a strengthening in the EMS, the EMDW O_2 concentration after 100 years is 23–32 μM (12–17%) higher than in the baseline simulation. Over the same time period, the WMDW O_2 concentration decreases by 12–21 μM (6–10%). As a result, the WMDW O_2 concentration drops below that of the WMIW, in contrast to the baseline simulation where the WMIW exhibits a lower O_2 concentration than both the WMSW and WMDW.

Strengthening of the THC in both WMS and EMS in scenario WC3.1 increases the O_2 DW concentration of the EMS. For the WMDW, the decrease in O_2 SW solubility and faster degradation kinetics offset the effect of increased ventilation. Hence, despite the 74% increase in WMDW formation, the WMDW O_2 concentration only changes by approximately 3% relative to the baseline results. Overall, the changes in SW O_2 solubility and aerobic degradation kinetics due to climate warming buffer the potential increases in DW O_2 concentrations associated with enhanced DW formation in WC2.1 and WC3.1, while they enhance the decline in O_2 concentrations due to slower DW formation in WC1.1. The results discussed so far are based on applying equation (1) to both IW and DW. That is, they assume that O_2 consumption rates only respond to changes in O_2 concentration. The EMT and WMT simulations, however, imply that changes in THC also affect the supply of degradable DOC to the DW reservoirs (section 4.2). Therefore, the MS may exhibit a DOC-based negative feedback mechanism on DW oxygenation. As shown in Figure 5, using equation (2) in the circulation scenarios (i.e., scenarios WC1.2, WC2.2, and WC3.2) substantially reduces the predicted

ranges of the responses of DW O_2 concentrations to the imposed changes in THC. This is particularly the case in WC1.2 where after 100 years the WMDW and EMDW O_2 concentrations decrease to 178–183 and 171–172 μM , respectively, compared to 151–158 and 160–162 μM using equation (1) (Figure 4). Likewise, in WC3.2 enhanced THC across the entire MS supplies more degradable DOC to the DW, leading to an increase in O_2 consumption and, hence, lower DW O_2 concentrations than those predicted in WC3.1.

Factors other than those considered here will undoubtedly affect the future trends of water column O_2 levels in the MS. In particular, future increases in anthropogenic nutrients inputs into the MS [Ludwig *et al.*, 2010; Lazzari *et al.*, 2014; Christodoulaki *et al.*, 2016; Powley *et al.*, 2016] may promote higher primary productivity in the SWs, which in turn would enhance O_2 consumption in the IW and DW reservoirs. Furthermore, our model results only pertain to basin-wide O_2 trends in the offshore IW and DW masses of the MS. Increased local nutrient supply, together with lower O_2 solubility and faster respiration rates, have the potential to enhance hypoxia in a limited number of nearshore areas around the MS basin.

4.3.2. Long-Term Responses (>100 Years)

The timescales over which DW O_2 concentrations respond to the imposed circulation changes in WC2 and WC3 are ≤ 50 years (Figure 4). In contrast, the response times in WC1 exceed 115 years for WMDW and 500 years for EMDW. Thus, we expect relatively slow adjustments of the DW O_2 concentrations to a generalized drop in DW formation, especially in the EMS. For EMDW O_2 concentrations to drop within 1 μM of the steady state values requires more than 1300 years in scenario WC1.1, and 3400 years in scenario WC1.2. Furthermore, although the EMDW O_2 concentrations in WC1.1 and WC1.2 decrease to steady state values of 11–47 μM , the WMDW retains O_2 concentrations well above 100 μM (Figure 4). On long timescales, EMDW is thus more sensitive to O_2 depletion caused by a weakening of the THC than WMDW, in contrast to the behavior observed at shorter timescales (section 4.3.1).

The weakened and shallower THC in scenario WC1 is not unlike the circulation regime inferred for sapropel formation in the EMS, despite the probably very different—cooler and wetter—climate conditions [Rohling *et al.*, 2015]. Grimm *et al.* [2015] propose that the formation of sapropel S1 was preceded by thousands of years of preconditioning of the water masses following DW stagnation, that is, similar to the timescales

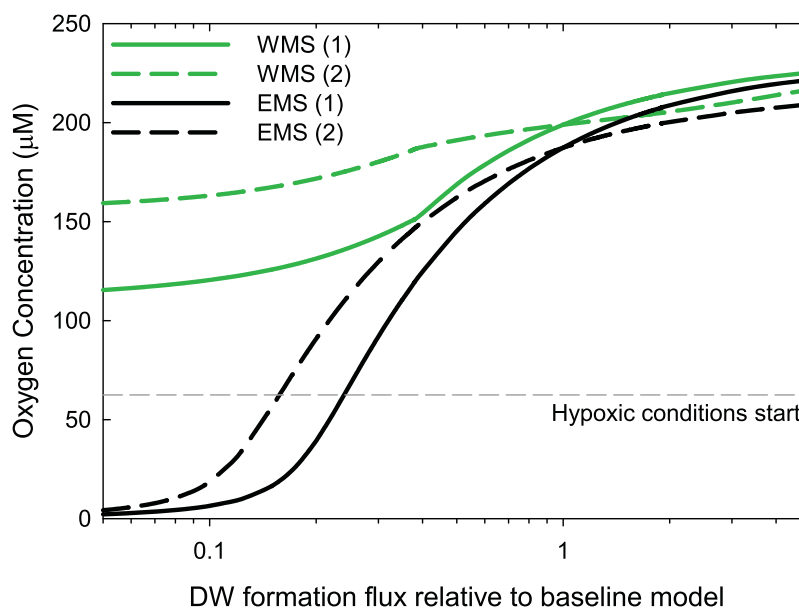


Figure 6. Steady state DW O_2 concentrations as a function of the DW formation rates in the EMS (from the Adriatic and Aegean Seas) and WMS (from the NWM and Tyrrhenian Sea), relative to the baseline (pre-EMT) rates. Numbers in brackets correspond to the equation used for DW O_2 consumption rates: equation (1) or equation (2). The calculations assume that the contribution of Bernoulli suction of WMDW to total outflow at the Strait of Gibraltar remains constant at 30%, while upwelling fluxes from DW to IW (F_{65} and F_{32} in Figure 1) are adjusted to maintain steady state. In the WMS, the F_{32} flux switches from upwelling to downwelling when the DW formation flux drops below 37% of its pre-EMT value. Note a reduction in the DW formation flux to 0.15 and 0.26 relative to the baseline model in the EMS and WMS, respectively, correspond to the reduction imposed in WC1.

required by EMDW to approach hypoxic conditions in the WC1 simulations. Other authors have proposed that only a massive, long-term change in THC, such as a reversal of the antiestuarine circulation, could have produced anoxia in the EMS [Sarmiento *et al.*, 1988; Stratford *et al.*, 2000]. In line with the WC1 results, the available evidence indicates that DW O₂ concentrations in the WMS remained relatively high at the same time that sapropels were being deposited under the O₂-depleted DW of the EMS. Rohling *et al.* [2015] hypothesize that WMDW remained oxygenated because of the efficient removal of old WMDW by Bernoulli suction through the Strait of Gibraltar, while this mechanism was absent at the Strait of Sicily.

The sensitivity of WMDW and EMDW oxygenation to the rates of DW formation is summarized in Figure 6. Steady state O₂ concentrations of WMDW and EMDW are plotted as a function of the relative rates of DW formation in the WMS and EMS. The figure shows that all other conditions equal: (1) only the EMDW can develop hypoxia, but not the WMDW; (2) the inclusion of the DOC-based negative feedback dampens the response of the O₂ concentrations to changes in DW formation; and (3) the rate of EMDW formation must drop to at least 24% of its pre-EMT value in order to develop basin-wide DW hypoxic conditions in the EMS. The figure also implies that changes in the long-term rates of WMDW and EMDW formation by factors of ± 2 should have relatively limited impact on the average DW O₂ concentrations ($\leq 25\%$ change). In other words, DW oxygenation of the MS appears to be fairly resilient to potential changes in circulation that may occur in the foreseeable future.

5. Conclusions

A mass balance modeling approach is used to assess the sensitivity of IW and DW O₂ distributions in the MS to climate-driven changes in O₂ solubility, organic matter degradation kinetics, and THC. The present-day O₂ distributions are based on a simplified representation of the water cycle that incorporates the most recent flow estimates through the Strait of Gibraltar. The model yields O₂ consumption rates in the various reservoirs of the WMS and EMS that fall within the ranges of reported values. Prior to the EMT, EMIW exhibits approximately 2 times faster O₂ consumption than WMIW, while the O₂ consumption rate is 2.5 times greater in WMDW than EMDW. In order to reproduce the general trends in O₂ concentrations and consumption observed during and after the EMT and WMT, the model must account for the variations in labile DOC influxes to the WMDW and EMDW associated with changes in DW formation. The coupling between the delivery of O₂ and DOC to the DW reservoirs creates a negative feedback that dampens the magnitude of the changes in DW O₂ concentrations that accompany changes in THC.

In the climate change scenarios, the predicted variations in O₂ concentrations of WMDW and EMDW are most strongly affected by changes in water circulation: the imposed perturbations to the THC change DW O₂ concentrations by up to 25% within 100 years, compared to the maximum changes of 7 and 2% for the imposed decreases in O₂ solubility and aerobic respiration kinetics, respectively. Even after 100 years of strongly reduced DW formation, the WMS and EMS are predicted to stay fully oxygenated. On time-scales of several thousands of years, a sustained decrease in THC of 75% or more relative to today would result in hypoxic bottom waters in the EMS. The average WMDW O₂ concentration, however, would still remain above 110 μM , because Bernoulli suction through the Strait of Gibraltar keeps the WMDW reservoir well ventilated. Overall, while the model results imply that climate warming in the Mediterranean region will significantly impact water column O₂ cycling, it is unlikely to cause basin-wide bottom water hypoxia within the 21st century. Note, however, that the predicted changes in O₂ distributions do not account for additional factors that may affect O₂ consumption rates, in particular, rising inputs of anthropogenic nutrients to the MS.

A key limitation of our ability to forecast the effects of climate-driven changes in THC on the biogeochemical functioning of the MS are the large uncertainties surrounding not only the magnitude of the potential circulation changes, but also their direction. As the recent study of Adloff *et al.* [2015] illustrates, even the question whether future climate warming will strengthen or weaken THC in the MS has yet to be satisfactorily answered. As emphasized by our mass balance results, monitoring the changes in the water column O₂ distributions can yield powerful insights into the coupling between the geophysical and ecological dynamics of the MS and their response to climate forcing.

Acknowledgments

We thank the Editor, Peter Brewer, and two anonymous reviewers for their constructive comments on the manuscript, and Paul Myers and Hans Dürr for useful discussions on modeling the Mediterranean circulation. This work was funded by the Canada Excellence Research Chair (CERC) Program. All data for this paper are properly cited and referred to in the reference list and presented in figures and table of this manuscript and Supporting Information. The source code for this study is available from the authors upon request (hrpowley@uwaterloo.ca).

References

Adloff, F., et al. (2015), Mediterranean Sea response to climate change in an ensemble of twenty first century scenarios, *Clim. Dyn.*, *45*, 2775–2802, doi:10.1007/s00382-015-2507-3.

Altieri, A. H., and K. B. Gedan (2015), Climate change and dead zones, *Global Change Biol.*, *21*(4), 1395–1406, doi:10.1111/gcb.12754.

Antoine, D., A. Morel, and J.-M. André (1995), Algal pigment distribution and primary production in the eastern Mediterranean as derived from coastal zone color scanner observations, *J. Geophys. Res.*, *100*(C8), 16,193–16,209, doi:10.1029/95JC00466.

Bergamasco, A., and P. Malanotte-Rizzoli (2010), The circulation of the Mediterranean Sea: A historical review of experimental investigations, *Adv. Oceanogr. Limnol.*, *1*(1), 11–28, doi:10.1080/19475721.2010.491656.

Béthoux, J. P., and B. Gentili (1999), Functioning of the Mediterranean Sea: Past and present changes related to freshwater input and climate changes, *J. Mar. Syst.*, *20*(1–4), 33–47, doi:10.1016/S0924-7963(98)00069-4.

Béthoux, J. P., B. Gentili, J. Raunet, and D. Tailliez (1990), Warming trend in the Western Mediterranean Deep-Water, *Nature*, *347*(6294), 660–662, doi:10.1038/347660a0.

Béthoux, J. P., P. Morin, C. Madec, and B. Gentili (1992), Phosphorus and nitrogen behavior in the Mediterranean Sea, *Deep Sea Res., Part A*, *39*(9A), 1641–1654.

Béthoux, J. P., X. D. de Madron, F. Nyffeler, and D. Tailliez (2002), Deep water in the western Mediterranean: Peculiar 1999 and 2000 characteristics, shelf formation hypothesis, variability since 1970 and geochemical inferences, *J. Mar. Syst.*, *33*, 117–131, doi:10.1016/S0924-7963(02)00055-6.

Bianchi, M., C. Fosset, and P. Conan (1999), Nitrification rates in the NW Mediterranean Sea, *Aquat. Microb. Ecol.*, *17*(3), 267–278, doi:10.3354/ame017267.

Borghini, M., H. Bryden, K. Schroeder, S. Sparnocchia, and A. Vetrano (2014), The Mediterranean is becoming saltier, *Ocean Sci.*, *10*(4), 693–700, doi:10.5194/os-10-693-2014.

Box, G. E. P., W. G. Hunter, and J. S. Hunter (1978), *Statistics for Experimenters. An Introduction to Design, Data Analysis and Model Building*, 653 pp., John Wiley, New York.

Brewer, P. G., and E. T. Peltzer (2016), Ocean chemistry, ocean warming, and emerging hypoxia: Commentary, *J. Geophys. Res. Oceans*, *121*, 3659–3667, doi:10.1002/2016JC011651.

Bryden, H. L., J. Candela, and T. H. Kinder (1994), Exchange through the Strait of Gibraltar, *Prog. Oceanogr.*, *33*(3), 201–248, doi:10.1016/0079-6611(94)90028-0.

Carstensen, J., J. H. Andersen, B. G. Gustafsson, and D. J. Conley (2014), Deoxygenation of the Baltic Sea during the last century, *Proc. Natl. Acad. Sci. U. S. A.*, *111*(15), 5628–5633, doi:10.1073/pnas.1323156111.

Christensen, J. P., T. T. Packard, F. Q. Dortch, H. J. Minas, J. C. Gascard, C. Richez, and P. C. Garfield (1989), Carbon oxidation in the deep Mediterranean Sea: Evidence for dissolved organic carbon source, *Global Biogeochem. Cycles*, *3*(4), 315–335, doi:10.1029/GB003i004p00315.

Christodoulaki, S., G. Petihakis, N. Mihalopoulos, K. Tsiaras, G. Triantafyllou, and M. Kanakidou (2016), Human-driven atmospheric deposition of N and P controls on the east Mediterranean marine ecosystem, *J. Atmos. Sci.*, *73*(4), 1611–1619, doi:10.1175/jas-d-15-0241.1.

Collins, M., et al. (2013), Long-term climate change: Projections, commitments and irreversibility, in *Climate Change 2013: The Physical Science Basis. Contribution of Working Group I to the Fifth Assessment Report of the Intergovernmental Panel on Climate Change*, edited by T. F. Stocker et al., pp. 1029–1136, Cambridge Univ. Press, Cambridge, U. K.

Copin-Montégut, C. (2000), Consumption and production on scales of a few days of inorganic carbon, nitrate and oxygen by the planktonic community: Results of continuous measurements at the Dyfamed Station in the northwestern Mediterranean Sea (May 1995), *Deep Sea Res., Part I*, *47*(3), 447–477, doi:10.1016/S0967-0637(99)00098-9.

Criado-Aldeanueva, F., F. J. Soto-Navarro, and J. García-Lafuente (2012), Seasonal and interannual variability of surface heat and freshwater fluxes in the Mediterranean Sea: Budgets and exchange through the Strait of Gibraltar, *Int. J. Climatol.*, *32*(2), 286–302, doi:10.1002/joc.2268.

Cuyppers, Y., P. Bouruet-Aubertot, C. Marec, and J. L. Fuda (2012), Characterization of turbulence from a fine-scale parameterization and microstructure measurements in the Mediterranean Sea during the BOUM experiment, *Biogeosciences*, *9*(8), 3131–3149, doi:10.5194/bg-9-3131-2012.

de Madron, X. D., V. Zervakis, A. Theocharis, and D. Georgopoulos (2005), Comments on “Cascades of dense water around the world ocean,” *Prog. Oceanogr.*, *64*(1), 83–90, doi:10.1016/j.pocean.2004.08.004.

de Madron, X. D., et al. (2013), Interaction of dense shelf water cascading and open-sea convection in the northwestern Mediterranean during winter 2012, *Geophys. Res. Lett.*, *40*, 1379–1385, doi:10.1002/grl.50331.

Doney, S. C., et al. (2012), Climate change impacts on marine ecosystems, *Annu. Rev. Mar. Sci.*, *4*, 11–37.

Flecha, S., F. F. Perez, J. Garcia-Lafuente, S. Sammartino, A. F. Rios, and I. Emma Huertas (2015), Trends of pH decrease in the Mediterranean Sea through high frequency observational data: Indication of ocean acidification in the basin, *Sci. Rep.*, *5*, Article 16770, doi:10.1038/srep16770.

Forryan, A., J. T. Allen, E. Edhouse, B. Silburn, K. Reeve, and E. Tesi (2012), Turbulent mixing in the eddy transport of Western Mediterranean Intermediate Water to the Alboran Sea, *J. Geophys. Res.*, *117*, C09008, doi:10.1029/2012JC008284.

Friedrich, J., et al. (2014), Investigating hypoxia in aquatic environments: Diverse approaches to addressing a complex phenomenon, *Biogeosciences*, *11*(4), 1215–1259, doi:10.5194/bg-11-1215-2014.

Fuda, J. L., C. Millot, I. Taupier-Letage, U. Send, and J. M. Bocognano (2000), XBT monitoring of a meridian section across the western Mediterranean Sea, *Deep Sea Res., Part I*, *47*(11), 2191–2218, doi:10.1016/S0967-0637(00)00018-2.

García Lafuente, J., A. Sánchez Román, G. Díaz del Río, G. Sannino, and J. C. Sánchez Garrido (2007), Recent observations of seasonal variability of the Mediterranean outflow in the Strait of Gibraltar, *J. Geophys. Res.*, *112*, C10005, doi:10.1029/2006JC003992.

Gasparini, G. P., A. Ortona, G. Budillon, M. Astraldi, and E. Sansone (2005), The effect of the Eastern Mediterranean Transient on the hydrographic characteristics in the Strait of Sicily and in the Tyrrhenian Sea, *Deep Sea Res., Part I*, *52*(6), 915–935, doi:10.1016/j.dsr.2005.01.001.

Giorgi, F. (2006), Climate change hot-spots, *Geophys. Res. Lett.*, *33*, L08707, doi:10.1029/2006GL025734.

Grimm, R., E. Maier-Reimer, U. Mikolajewicz, G. Schmiedl, K. Mueller-Navarra, F. Adloff, K. M. Grant, M. Ziegler, L. J. Lourens, and K.-C. Emeis (2015), Late glacial initiation of Holocene eastern Mediterranean sapropel formation, *Nat. Commun.*, *6*, Article 7099, doi:10.1038/ncomms8099.

Gualdi, S., et al. (2013), The CIRCE simulations: Regional climate change projections with realistic representation of the Mediterranean Sea, *Bull. Am. Meteorol. Soc.*, *94*(1), 65–81, doi:10.1175/bams-d-11-00136.1.

- Herrmann, M., C. Estournel, M. Déqué, P. Marsaleix, F. Sevault, and S. Somot (2008), Dense water formation in the Gulf of Lions shelf: Impact of atmospheric interannual variability and climate change, *Cont. Shelf Res.*, 28(15), 2092–2112, doi:10.1016/j.csr.2008.03.003.
- Kirtman, B., et al. (2013), Near-term climate change: Projections and predictability, in *Climate Change 2013: The Physical Science Basis. Contribution of Working Group I to the Fifth Assessment Report of the Intergovernmental Panel on Climate Change*, edited by T. F. Stocker et al., pp. 953–1028, Cambridge Univ. Press, Cambridge, U. K.
- Klein, B., W. Roether, B. B. Manca, D. Bregant, V. Beitzel, V. Kovacevic, and A. Luchetta (1999), The large deep water transient in the Eastern Mediterranean, *Deep Sea Res., Part I*, 46(3), 371–414.
- Klein, B., W. Roether, N. Kress, B. B. Manca, M. R. d'Alcala, E. Souvermezoglou, A. Theocharis, G. Civitarese, and A. Luchetta (2003), Accelerated oxygen consumption in eastern Mediterranean deep waters following the recent changes in thermohaline circulation, *J. Geophys. Res.*, 108(C9), 8107, doi:10.1029/2002JC001454.
- Kress, N., B. B. Manca, B. Klein, and D. Deponte (2003), Continuing influence of the changed thermohaline circulation in the eastern Mediterranean on the distribution of dissolved oxygen and nutrients: Physical and chemical characterization of the water masses, *J. Geophys. Res.*, 108(C9), 8109, doi:10.1029/2002JC001397.
- Kress, N., H. Herut, and I. Gertman (2012), Nutrient distribution in the Eastern Mediterranean before and after the Transient Event, in *Life in the Mediterranean Sea: A Look at Habitat Changes*, edited by N. Stambler, pp. 157–174, Nova Sci. Publ., New York.
- Kress, N., I. Gertman, and B. Herut (2014), Temporal evolution of physical and chemical characteristics of the water column in the Easternmost Levantine basin (Eastern Mediterranean Sea) from 2002 to 2010, *J. Mar. Syst.*, 135, 6–13, doi:10.1016/j.jmarsys.2013.11.016.
- Lazzari, P., G. Mattia, C. Solidoro, S. Salon, A. Crise, M. Zavatarelli, P. Oddo, and M. Vichi (2014), The impacts of climate change and environmental management policies on the trophic regimes in the Mediterranean Sea: Scenario analyses, *J. Mar. Syst.*, 135, 137–149, doi:10.1016/j.jmarsys.2013.06.005.
- Lefèvre, D., M. Denis, C. E. Lambert, and J. C. Miquel (1996), Is DOC the main source of organic matter remineralization in the ocean water column?, *J. Mar. Syst.*, 7(2–4), 281–291, doi:10.1016/0924-7963(95)00003-8.
- L'Hévéder, B., L. Li, F. Sevault, and S. Somot (2013), Interannual variability of deep convection in the Northwestern Mediterranean simulated with a coupled AORCM, *Clim. Dyn.*, 41(3–4), 937–960, doi:10.1007/s00382-012-1527-5.
- Ludwig, W., E. Dumont, M. Meybeck, and S. Heussner (2009), River discharges of water and nutrients to the Mediterranean and Black Sea: Major drivers for ecosystem changes during past and future decades?, *Prog. Oceanogr.*, 80(3–4), 199–217, doi:10.1016/j.pocean.2009.02.001.
- Ludwig, W., A. F. Bouwman, E. Dumont, and F. Lespinas (2010), Water and nutrient fluxes from major Mediterranean and Black Sea rivers: Past and future trends and their implications for the basin-scale budgets, *Global Biogeochem. Cycles*, 24, GB0A13, doi:10.1029/2009GB003594.
- Luna, G. M., S. Bianchelli, F. Decembrini, E. De Domenico, R. Danovaro, and A. Dell'Anno (2012), The dark portion of the Mediterranean Sea is a bioreactor of organic matter cycling, *Global Biogeochem. Cycles*, 26, GB2017, doi:10.1029/2011GB004168.
- Marty, J. C., and J. Chiaverini (2010), Hydrological changes in the Ligurian Sea (NW Mediterranean, DYFAMED site) during 1995–2007 and biogeochemical consequences, *Biogeosciences*, 7(7), 2117–2128, doi:10.5194/bg-7-2117-2010.
- MEDAR Group (2002), *MEDATLAS/2002 Database. Mediterranean and Black Sea Database of Temperature Salinity and Bio-Chemical Parameters—Climatological Atlas*, IFREMER / IDM / SISMER - Scientific Information Systems for the SEA, Plouzane, France.
- Medoc Group (1970), Observation of formation of deep water in the Mediterranean Sea, 1969, *Nature*, 227, 1037–1040.
- Millot, C. (1999), Circulation in the Western Mediterranean Sea, *J. Mar. Syst.*, 20(1–4), 423–442, doi:10.1016/S0924-7963(98)00078-5.
- Millot, C. (2009), Another description of the Mediterranean Sea outflow, *Prog. Oceanogr.*, 82(2), 101–124, doi:10.1016/j.pocean.2009.04.016.
- Millot, C. (2014), Heterogeneities of in- and out-flows in the Mediterranean Sea, *Prog. Oceanogr.*, 120, 254–278, doi:10.1016/j.pocean.2013.09.007.
- Moutin, T., and P. Raimbault (2002), Primary production, carbon export and nutrients availability in western and eastern Mediterranean Sea in early summer 1996 (MINOS cruise), *J. Mar. Syst.*, 33, 273–288, doi:10.1016/S0924-7963(02)00062-3.
- Planton, S., et al. (2012), The climate of mediterranean region in future climate projections, in *The Climate of the Mediterranean Region: From the Past to the Future*, edited by P. Lionello, pp. 449–205, Elsevier, Amsterdam.
- Powley, H. R., M. D. Krom, K.-C. Emeis, and P. Van Cappellen (2014), A biogeochemical model for phosphorus and nitrogen cycling in the Eastern Mediterranean Sea (EMS) Part 2. Response of nutrient cycles and primary production to anthropogenic forcing: 1950–2000, *J. Mar. Syst.*, 139, 420–432.
- Powley, H. R., H. H. Dürr, A. T. Lima, M. D. Krom, and P. Van Cappellen (2016), Direct discharges of domestic wastewater are a major source of phosphorus and nitrogen to the Mediterranean Sea, *Environ. Sci. Technol.*, 50, 8722–8730, doi:10.1021/acs.est.6b01742.
- Rabalais, N. N., R. J. Diaz, L. A. Levin, R. E. Turner, D. Gilbert, and J. Zhang (2010), Dynamics and distribution of natural and human-caused hypoxia, *Biogeosciences*, 7(2), 585–619.
- Rhein, M. (1995), Deep water formation in the western Mediterranean, *J. Geophys. Res.*, 100(C4), 6943–6959, doi:10.1029/94JC03198.
- Rixen, M., et al. (2005), The Western Mediterranean Deep Water: A proxy for climate change, *Geophys. Res. Lett.*, 32, 47–50, doi:10.1029/2005GL022702.
- Roether, W., and J. E. Lupton (2011), Tracers confirm downward mixing of Tyrrhenian Sea upper waters associated with the Eastern Mediterranean Transient, *Ocean Sci.*, 7(1), 91–99, doi:10.5194/os-7-91-2011.
- Roether, W., and R. Well (2001), Oxygen consumption in the Eastern Mediterranean, *Deep Sea Res., Part I*, 48(6), 1535–1551.
- Roether, W., B. B. Manca, B. Klein, D. Bregant, D. Georgopoulos, V. Beitzel, V. Kovacevic, and A. Luchetta (1996), Recent changes in eastern Mediterranean deep waters, *Science*, 271(5247), 333–335.
- Roether, W., B. Klein, B. B. Manca, A. Theocharis, and S. Kioroglou (2007), Transient Eastern Mediterranean deep waters in response to the massive dense-water output of the Aegean Sea in the 1990s, *Prog. Oceanogr.*, 74, 540–571, doi:10.1016/j.pocean.2007.001.
- Rohling, E. J., G. Marino, and K. M. Grant (2015), Mediterranean climate and oceanography, and the periodic development of anoxic events (sapropels), *Earth Sci. Rev.*, 143, 62–97, doi:10.1016/j.earscirev.2015.01.008.
- Sánchez-Román, A., G. Sannino, J. García-Lafuente, A. Carrillo, and F. Criado-Aldeanueva (2009), Transport estimates at the western section of the Strait of Gibraltar: A combined experimental and numerical modeling study, *J. Geophys. Res.*, 114, C06002, doi:10.1029/2008JC005023.
- Santinelli, C. (2015), DOC in the Mediterranean Sea, in *Biogeochemistry of Marine Dissolved Organic Matter*, edited by D. A. Hansell and C. A. Carlson, pp. 579–608, Academic Press, London, U. K.
- Santinelli, C., L. Nannicini, and A. Seritti (2010), DOC dynamics in the meso and bathypelagic layers of the Mediterranean Sea, *Deep Sea Res., Part II*, 57(16), 1446–1459, doi:10.1016/j.dsr2.2010.02.014.

- Santinelli, C., R. Sempéré, F. Van Wambeke, B. Charriere, and A. Seritti (2012), Organic carbon dynamics in the Mediterranean Sea: An integrated study, *Global Biogeochem. Cycles*, *26*, GB4004, doi:10.1029/2011GB004151.
- Sarmiento, J. L., T. Herbert, and J. R. Toggweiler (1988), Mediterranean nutrient balance and episodes of anoxia, *Global Biogeochem. Cycles*, *2*(4), 427–444.
- Savenkoff, C., L. Prieur, J. P. Reys, D. Lefevre, S. Dallot, and M. Denis (1993), Deep microbial communities evidenced in the Liguro-Provençal front by their ETS activity, *Deep Sea Res., Part I*, *40*(4), 709–725, doi:10.1016/0967-0637(93)90067-d.
- Schneider, A., T. Tanhua, W. Roether, and R. Steinfeldt (2014), Changes in ventilation of the Mediterranean Sea during the past 25 year, *Ocean Sci.*, *10*(1), 1–16, doi:10.5194/os-10-1-2014.
- Schroeder, K., G. P. Gasparini, M. Tangherlini, and M. Astraldi (2006), Deep and intermediate water in the western Mediterranean under the influence of the Eastern Mediterranean Transient, *Geophys. Res. Lett.*, *33*, L21607, doi:10.1029/2006GL027121.
- Schroeder, K., M. Borghini, G. Cerrati, V. Difesca, R. Delfanti, C. Santinelli, and G. P. Gasparini (2008a), Multiparametric mixing analysis of the deep waters in the Western Mediterranean Sea, *Chem. Ecol.*, *24*(suppl. 1), 47–56, doi:10.1080/02757540801970373.
- Schroeder, K., A. Ribotti, M. Borghini, R. Sorgente, A. Perilli, and G. P. Gasparini (2008b), An extensive western Mediterranean deep water renewal between 2004 and 2006, *Geophys. Res. Lett.*, *35*, L18605, doi:10.1029/2008GL035146.
- Schroeder, K., V. Taillandier, A. Vetrano, and G. P. Gasparini (2008c), The circulation of the western Mediterranean Sea in spring 2005 as inferred from observations and from model outputs, *Deep Sea Res., Part I*, *55*(8), 947–965, doi:10.1016/j.dsr.2008.04.003.
- Somot, S., F. Sevault, and M. Déqué (2006), Transient climate change scenario simulation of the Mediterranean Sea for the twenty-first century using a high-resolution ocean circulation model, *Clim. Dyn.*, *27*(7–8), 851–879, doi:10.1007/s00382-006-0167-z.
- Soto-Navarro, J., F. Criado-Aldeanueva, J. García-Lafuente, and A. Sánchez-Román (2010), Estimation of the Atlantic inflow through the Strait of Gibraltar from climatological and in situ data, *J. Geophys. Res.*, *115*, C10023, doi:10.1029/2010JC006302.
- Stratford, K., R. G. Williams, and P. G. Drakopoulos (1998), Estimating climatological age from a model-derived oxygen-age relationship in the Mediterranean, *J. Mar. Syst.*, *18*(1–3), 215–226, doi:10.1016/s0924-7963(98)00013-x.
- Stratford, K., R. G. Williams, and P. G. Myers (2000), Impact of the circulation on sapropel formation in the eastern Mediterranean, *Global Biogeochem. Cycles*, *14*(2), 683–695, doi:10.1029/1999GB001157.
- Takahashi, T., W. S. Broecker, and S. Langer (1985), Redfield ratio based on chemical-data from isopycnal surfaces, *J. Geophys. Res.*, *90*(NC4), 6907–6924, doi:10.1029/JC090iC04p06907.
- Tanaka, T., and F. Rassoulzadegan (2004), Vertical and seasonal variations of bacterial abundance and production in the mesopelagic layer of the NW Mediterranean Sea: Bottom-up and top-down controls, *Deep Sea Res., Part I*, *51*(4), 531–544, doi:10.1016/j.dsr.2003.12.001.
- Testa, J. M., Y. Li, Y. J. Lee, M. Li, D. C. Brady, D. M. Di Toro, W. M. Kemp, and J. J. Fitzpatrick (2014), Quantifying the effects of nutrient loading on dissolved O₂ cycling and hypoxia in Chesapeake Bay using a coupled hydrodynamic–biogeochemical model, *J. Mar. Syst.*, *139*, 139–158, doi:10.1016/j.jmarsys.2014.05.018.
- Thorpe, R. B., and G. R. Bigg (2000), Modelling the sensitivity of Mediterranean Outflow to anthropogenically forced climate change, *Clim. Dyn.*, *16*(5), 355–368, doi:10.1007/s003820050333.
- Ulses, C., C. Estournel, P. Puig, X. D. de Madron, and P. Marsaleix (2008), Dense shelf water cascading in the northwestern Mediterranean during the cold winter 2005: Quantification of the export through the Gulf of Lion and the Catalan margin, *Geophys. Res. Lett.*, *35*, L07610, doi:10.1029/2008GL033257.
- Van Cappellen, P., H. R. Powley, K.-C. Emeis, and M. D. Krom (2014), A biogeochemical model for phosphorus and nitrogen cycling in the Eastern Mediterranean Sea (EMS). Part 1. Model development, initial conditions and sensitivity analyses, *J. Mar. Syst.*, *139*, 460–471.
- Vargas-Yáñez, M., P. Zunino, K. Schroeder, J. L. López-Jurado, F. Plaza, M. Serra, C. Castro, M. C. García-Martínez, F. Moya, and J. Salat (2012), Extreme Western Intermediate Water formation in winter 2010, *J. Mar. Syst.*, *105–108*, 52–59, doi:10.1016/j.jmarsys.2012.05.010.
- Vichi, M., et al. (2015), The biogeochemical flux model (BFM): Equation description and user manual, BFM version 5.1, in *BFM Rep. Ser. 1*, Release 1.1, pp. 104, Biogeochem., Flux Model, Bologna, Italy. [Available at <http://bfm-community.eu>.]
- Williams, P. J. L. B. (2014), Plankton respiration, net community production and the organic carbon cycle in the oceanic water column A2—Holland, Heinrich D, in *Treatise on Geochemistry*, 2nd ed., edited by K. K. Turekian, pp. 593–612, Elsevier, Oxford, U. K.
- Zekster, I. S., R. G. Dzhamalov, and L. G. Everett (2007), *Submarine Groundwater*, Taylor & Francis, Fla.
- Zhai, W. D., H. D. Zhao, N. Zheng, and Y. Xu (2012), Coastal acidification in summer bottom oxygen-depleted waters in northwestern-northern Bohai Sea from June to August in 2011, *Chin. Sci. Bull.*, *57*(9), 1062–1068, doi:10.1007/s11434-011-4949-2.